Radar Tracking Enhancement Utilizing Target Size Estimation Based on the Range-Doppler Map

1st Mouhamed Aghiad Raslan
Dortmund University of Applied Sciences and Arts
Dortmund, Germany
mouhamed.raslan@fh-dortmund.de

2nd Rajab Murtaja
Dortmund University of Applied Sciences and Arts
Dortmund, Germany
rajab.murtaja@fh-dortmund.de

3rd Tobias Uhlich
Dortmund University of Applied Sciences and Arts
Dortmund, Germany
tobias.uhlich@fh-dortmund.de

4th Andreas Becker
Dortmund University of Applied Sciences and Arts
Dortmund, Germany
andreas.becker@fh-dortmund.de

***Abstract*—In advanced traffic safety systems, accurate vehicle tracking is crucial to improve road safety. However, in radar-based systems, 'glint noise,' caused by wandering reflection points on large vehicles such as trucks and buses, often poses a significant challenge by introducing errors in vehicle tracking. In this paper, we consider a radar-based traffic monitoring system, where such errors especially occur in situations involving large vehicles .**

This paper proposes an enhancement to tracking by leveraging a novel Range-Doppler-map-based method to mitigate glint noise effects, specifically for large vehicles. The core of our approach involves the size estimation of the target based on its signature on the Range-Doppler Map. By employing a Kalman Filter (KF), the proposed system simultaneously tracks both the position and the dynamically estimated size of vehicles, enabling more precise estimation of their movement. The proposed approach shows enhanced accuracy in tracking vehicles compared to commonly used methods. Our experimental results, based on measurements taken from a real-life traffic scenario, demonstrate the potential of this method to enhance the reliability of traffic monitoring systems.

***Index Terms*—KF, Traffic Radar, Tracking, Range-Doppler map, Vehicle size estimation.**

I. Introduction

The utilization of stationary radar systems for traffic safety monitoring has become significantly important, particularly in detecting and tracking both vehicles and Vulnerable Road Users (VRUs) such as pedestrians and cyclists. Radar sensors, specifically Millimeter-Wave (MMW) radars, have proven beneficial due to their resilience under various weather conditions and in visibility-limited scenarios [1], [2]. Despite numerous advancements, radar-based systems experience specific difficulties when observing large vehicles, specifically the phenomenon of glint noise. The glint noise arises due to multiple reflective surfaces, causing rapid fluctuations in radar reflections, which, in return, significantly complicates the accuracy of tracking relatively large vehicles such as trucks, buses, and articulated vehicles [3]. The impact of glint noise on radar data includes inconsistent measurement of target velocity, position, and tracking continuity, thus substantially impairing radar-based detection and tracking algorithms [4]. Studies have illustrated that the glint phenomenon of large vehicles also led to fragmented tracks and an increased false alarm rate, which ultimately reduces the reliability of the system [3].

Previous studies used different radar technologies, primarily Frequency-Modulated Continuous Wave (FMCW) radars, due to their effectiveness in measuring target range, velocity, and the angle of arrival [5]. In addition, signal processing techniques, including Kalman filtering and particle filtering methods, have been widely used to mitigate noise and improve tracking accuracy [3], [6]. Furthermore, researchers commonly combine radar sensing with complementary sensor technologies such as LiDAR or camera to improve the detections performance [7]. In addition, trained Artificial Intelligence (AI) models have recently been used, particularly in the field of target classification, for road safety and increased the reliability of radar monitoring systems [8].

A notable research gap identified in the reviewed literature is the insufficient development of dedicated algorithms and signal processing techniques specifically targeting glint noise reduction in tracking large vehicles. Although previous studies have highlighted glint-related tracking issues, they commonly employ standard filtering techniques, which may not fully resolve complex glint scenarios experienced in practical traffic environments [9].

In this paper, we are providing a novel method to overcome the glint noise in tracking large vehicles, utilizing solely the radar sensor, by estimating the target's length and width utilizing the Range-Doppler (RD) map, then incorporating the size information into the tracking algorithm. Afterwards, a camera-based ground truth system is used to verify the results.

The paper is constructed as follows: as this section (the introduction) presents the problem domain, section two, methodology, provides an explanation about the carried-out experi-

This study was based on data collected during working on the mFUND project "VIDETEC-2" and supported by Germany's Federal Minister for Digital and Transport under Grant 19F2232B.

ment, and the work-flow of the various data processing techniques. In the third section, results are presented that compare the accuracy of the proposed method with the traditional point-cloud tracking method, relative to the ground truth.

II. Methodology

The main focus of this paper is to reduce the glint effect caused by wandering reflections on large vehicles. A direct clustering approach is often used to cluster radar detections of a detected target based on different detections' criteria (spatial and/or velocity features) [10]. This method highly depends on the reflections' position along the target's body. Hence, estimating the target's dimensions can help reducing the abrupt fluctuations of the cluster's center caused by the glint noise. By pinpointing the obtained detections on the estimated size, and tracking both, the dimensions and the position of the target.

A. Experiment

The primary goal of tracking a vehicle approaching an intersection is to warn an oncoming driver of a potential collision with a VRU at a predicted time and location, often in the driver's blind spot (e.g., when both the vehicle and the VRU have the green light to turn right and to cross, respectively). VIDETEC-2 project addresses this critical scenario, by observing the intersection using radar sensors and Ultra-Wideband (UWB) nodes, then applying a target classification algorithm backed by a trained AI model [8]. After localizing and classifying the targets in the environment, a data fusion algorithm is applied to track the observed targets [11], in order to predict any potential danger that may fall onto the VRU, and in return, a warning signal is broadcasted to the vehicle [12]. Therefore, accurate vehicle tracking is critical; however, large vehicles such as trucks pose a challenge. Their considerable length and the effect of glint noise cause the center of the clustered detections to either fluctuate as seen in Fig. 1, or remain nearly stationary as they exit the radar's Field of View (FoV), degrading the prediction accuracy.

In this paper, we address this issue by introducing a novel pre-processing method for radar data, which is applied to the tracker to enhance its accuracy. The proposed algorithm is demonstrated using a case study of a long vehicle from real-life traffic, as shown in Fig. 1.

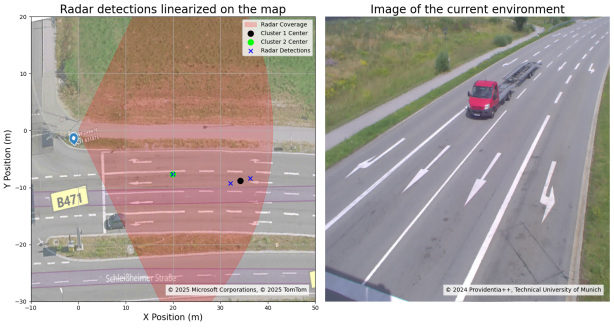

Fig. 1: A truck passing with very sparse detections, due to the glint noise, with detections and clusters centers.

The workflow of the proposed processing is broken down into the steps shown in the block diagram in Fig. 2.

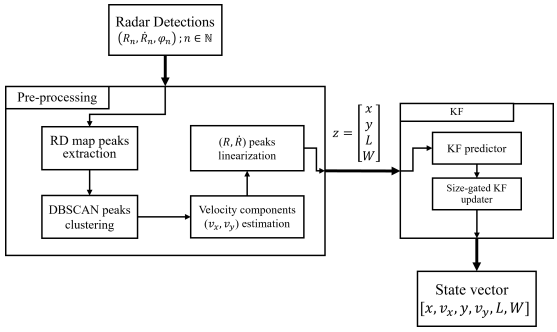

Fig. 2: A block diagram of the data pre-processing and tracking pipeline.

B. Size estimation

To estimate the target's size, based on its RD map distribution, several pre-processing operations are implemented:

1) RD-map peaks: a target, as large as a truck, appears on the RD map with a unique signature. This signature reveals some spatial feature that detections fail to provide, as seen in Fig. 3, where the detections of the target are located on the RD map, compared to the sub-peaks around them with slightly lower magnitude, they follow a certain pattern that can be useful for estimating the target's size.

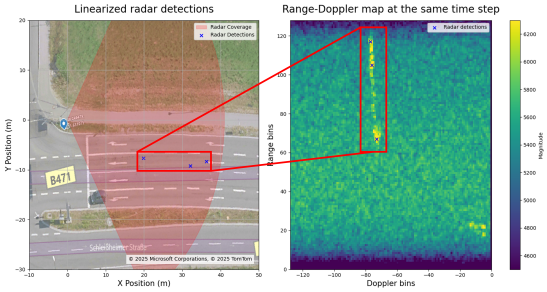

Fig. 3: The truck's signature on the RD map versus its detections showing the lack of spatial features obtained from the point cloud detections.

To extract these sub-peaks, a localized sub-peak detection algorithm is applied on the RD map, denoted as RDM $\in \mathbb{R}^{H \times W}$ (with H and W being the number of range and Doppler bins, respectively). For each radar detection located at coordinates $(r, \dot{r})$, we define a local Region of Interest (RoI) $\Omega_{r,\dot{r}}$ as the set of bins:

$$\Omega_{r,\dot{r}} = \{(u, v) \mid r - k \leq u \leq r + k,\ \dot{r} - k \leq v \leq \dot{r} + k\},$$

where u and v are the row (range) and column (radial velocity) indices within the local RoI, respectively, and k is the half-window size for a window of size $w \times w$ where $w = 2k + 1$.

Within the RoI $\Omega_{r,\dot{r}}$, the local mean $\mu_{r,\dot{r}}$ and the local standard deviation $\sigma_{r,\dot{r}}$ are calculated as

$$\mu_{r,\dot{r}} = \frac{1}{|\Omega_{r,\dot{r}}|} \sum_{(u,v)\in\Omega_{r,\dot{r}}} \text{RDM}(u,v),$$

$$\sigma_{r,\dot{r}} = \sqrt{\frac{1}{|\Omega_{r,\dot{r}}|-1} \sum_{(u,v)\in\Omega_{r,\dot{r}}} \Big(\text{RDM}(u,v) - \mu_{r,\dot{r}}\Big)^2},$$

with $|\Omega_{r,\dot{r}}|$ being the number of bins in the RoI [13]. An adaptive threshold $T_{r,\dot{r}}$ is then defined as

$$T_{r,\dot{r}} = \mu_{r,\dot{r}} + \alpha\,\sigma_{r,\dot{r}},$$

with α being a scaling factor that controls the selectivity of the threshold [14]. Within the RoI, any bin with the coordinates (u, v) that has a magnitude which exceeds this threshold and is a local maximum relative to its neighbors is considered a sub-peak. The collection of these sub-peaks, aggregated over all radar detections, provides additional information about the object's spatial extent while minimizing the influence of random noise.

2) clustering sub-peaks: since the extracted sub-peaks are around the radar detections, they form clusters, that are typically neighboring to each other on the RD map, in case the detections belong to a single target. Hence, a clustering algorithm is applied on the sub-peaks to bundle the different clusters together, and form a single, yet sizable, cluster. In this application, the Density-Based Spatial Clustering of Applications with Noise (DBSCAN) algorithm is applied on the RD map to cluster the regions with dense sub-peaks and form a relatively homogeneous shape of Range and Doppler bins, which in return could exploit the spatial features of the target.

3) Velocity components estimation: A radar detection point consists of the reflection point's range R, its angle of arrival ϕ, its elevation angle θ, and its radial velocity $\dot{R}$. The linearization process of such detections is commonly carried out as:

$$x = R\cos(\theta)\cos(\phi), \quad y = R\cos(\theta)\sin(\phi) \tag{1}$$

Nevertheless, since the radar sensor in this implementation is mounted on the side of the road, and the interest is focused only on the targets in the the x-y plane, the elevation angle is neglected in the linearization process.

Linearizing the measured radial velocity $\dot{R}$ can be derived from (2), by solving for the velocity components v_x and v_y in the cartesian coordinates.

$$\dot{R} = v_x\cos\phi + v_y\sin\phi \tag{2}$$

However, a combination of v_x and v_y yield to the same radial velocity $\dot{R}$, which means that v_x and v_y cannot be determined from a single pair of ($\dot{R}$, ϕ). Therefore, in case of a rigid object that reflects more than one detection, the true velocity components v_x and v_y can be calculated by the linear equations (3). By solving for v_x then substituting in (2).

$$v_y = \frac{\dot{R}_1}{\sin\phi_1} - \frac{v_x\cos\phi_1}{\sin\phi_1} = \frac{\dot{R}_2}{\sin\phi_2} - \frac{v_x\cos\phi_2}{\sin\phi_2} \tag{3}$$

4) sub-peaks linearization: the clustered sub-peaks can identify the range R and the radial velocity $\dot{R}$ of minor reflections on the target, yet they do not explicitly show the spatial coordinates of it, since the x-y coordinates of the target are calculated using (1), the ϕ information of the sub-peaks are missing. Therefore, equation (2) is used to restore the ϕ information, since these sub-peaks are estimated to be belonging to a single target, thanks to the clustering process. In addition, the values of v_x and v_y were previously calculated, which makes it possible to retrieve the ϕ information of each sub-peak. Fig. 4 shows the linearized sub-peaks in cartesian coordinates with a bounding box around them that could help in tracking the spatial properties of the target.

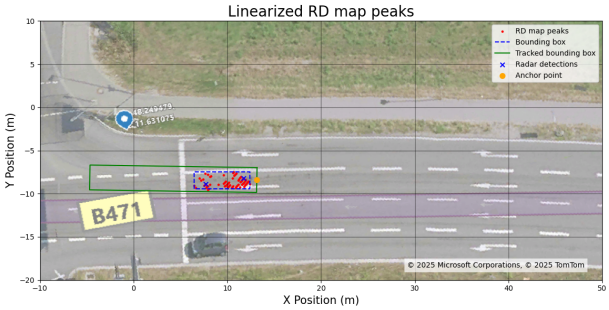

Fig. 4: The extracted peaks from the RD map are converted into Cartesian features along with the tracked bounding box.

C. Tracking

The main goal of the previously implemented preprocessing is to obtain not only a representation of an object in a shape of a single point, whether it is a cluster's center, or a single detection, but also the complete estimated size of the object, to improve tracking and prediction of the object's position in future time steps. However, the conventional approach of tracking a bounding box by using its centroid along with its dimensions and velocities [15] can lead to inaccuracies when the vehicle partially leaves the radar's field of view, as seen in Fig. 4, where its footprint shrinks and the centroid no longer represents the true center of the object.

Instead, the tracking algorithm uses an *anchor point*, which is the point opposite to the direction of movement (i.e., typically the rear of the vehicle) that remains visible longer in the FoV. Given the estimated cartesian velocity components, this anchor point can be estimated on the bounding box and used in the state vector to more reliably associate detections with the track. Once the clustered peaks are distilled into a bounding box with length L and width W, and an anchor point $(x_{\text{anchor}},\ y_{\text{anchor}})$, the measurement vector $\mathbf{z}$ is given by:

$$\mathbf{z} = [x_{\text{anchor}},\ y_{\text{anchor}},\ L,\ W] \tag{4}$$

Hence, a Kalman Filter is implemented to track the position and the size of the target, by integrating the estimated length and width of the observed object into the state vector $\mathbf{x}$ as in:

$$\mathbf{x} = [x, v_x, y, v_y, L, W]^T \tag{5}$$

where v_x and v_y are the cartesian velocity components. Using the same approach in [8] to determine the target's class, the values of L and W in the state vector $\mathbf{x}$ can be initialized with a predefined value according to the class.

For state prediction, a constant-velocity and constant-size model is adopted as $\mathbf{F}$, where the state propagation in the time step $k+1$ after a time Δt from the current state $\mathbf{x}_{k|k}$ is calculated as:

$$\mathbf{x}_{k+1|k} = \underbrace{\begin{bmatrix} 1 & \Delta t & 0 & 0 & 0 & 0 \\ 0 & 1 & 0 & 0 & 0 & 0 \\ 0 & 0 & 1 & \Delta t & 0 & 0 \\ 0 & 0 & 0 & 1 & 0 & 0 \\ 0 & 0 & 0 & 0 & 1 & 0 \\ 0 & 0 & 0 & 0 & 0 & 1 \end{bmatrix}}_{\mathbf{F}} \mathbf{x}_{k|k},$$

similarly, the predicted covariance propagation $\mathbf{P}_{k+1|k}$ of the current state's covariance $\mathbf{P}_{k|k}$ is given by:

$$\mathbf{P}_{k+1|k} = \mathbf{F}\,\mathbf{P}_{k|k}\,\mathbf{F}^T + \mathbf{Q},$$

where $\mathbf{Q}$ is the process noise accounting for small accelerations or size variations.

When a measurement is acquired, the update process starts, by defining a linear measurement model $\mathbf{z}_k$ for the anchor point and the target size observation:

$$\mathbf{z}_k = \underbrace{\begin{bmatrix} 1 & 0 & 0 & 0 & 0 & 0 \\ 0 & 0 & 1 & 0 & 0 & 0 \\ 0 & 0 & 0 & 0 & 1 & 0 \\ 0 & 0 & 0 & 0 & 0 & 1 \end{bmatrix}}_{\mathbf{H}} \mathbf{x}_{k|k-1} + \boldsymbol{\nu}_k, \quad \boldsymbol{\nu}_k \sim \mathcal{N}(\mathbf{0}, \mathbf{R}).$$

where $\mathbf{H}$ is the measurement matrix that links the tracker state to the preprocessed measurement, and $\mathbf{x}_{k|k-1}$ is the predicted (or a priori) state estimate before acquiring the measurement $\mathbf{z}_k$, and ν_k is the measurement noise related to the sensor inaccuracies.

By observing the radar data, it was noticed that large vehicles (e.g., trucks or those with trailers) take longer to fully enter and exit the radar's FoV. As such vehicles move into the FoV, an increasing portion becomes visible, while during exit, the observed vehicle size decreases. To address this discrepancy, the tracker incorporates a gating mechanism that compares the measured target's dimensions (length L and width W) with the corresponding values in the tracked state $\mathbf{x}$, which allows for the size to increase as the vehicle progresses into the FoV, and prevents it from shrinking while exiting the FoV, by inflating the corresponding diagonal elements of the measurement noise covariance matrix $\mathbf{R}$ to a large value to slow the update rate for L and W, preventing false size shrinkage and ensuring that the vehicle's true geometry is maintained in the tracker.

The Kalman filter update equations are given by [16]:

$$\mathbf{K}_k = \mathbf{P}_{k|k-1}\,\mathbf{H}^T\,(\mathbf{H}\,\mathbf{P}_{k|k-1}\,\mathbf{H}^T + \mathbf{R})^{-1},$$

$$\mathbf{x}_{k|k} = \mathbf{x}_{k|k-1} + \mathbf{K}_k\,(\mathbf{z}_k - \mathbf{H}\,\mathbf{x}_{k|k-1}),$$

$$\mathbf{P}_{k|k} = (\mathbf{I} - \mathbf{K}_k\,\mathbf{H})\,\mathbf{P}_{k|k-1}.$$

The Kalman gain $\mathbf{K}_k$ determines the weight assigned to the measurement residual $(\mathbf{z}_k - \mathbf{H}\,\mathbf{x}_{k|k-1})$, and $\mathbf{I}$ denotes the identity matrix. The updated (a posteriori) state estimate and its covariance are given by $\mathbf{x}_{k|k}$ and $\mathbf{P}_{k|k}$, respectively.

III. Results and Discussion

To assess the performance of the proposed approach, two evaluation methods are employed. First, the performance is compared against the traditional DBSCAN clustering algorithm applied to radar detections. Second, the Intersection over Union (IoU) metric and the center error metric are utilized to quantify the accuracy of the estimated bounding box.

A. Evaluation of Conventional DBSCAN

Experimental results indicate that even after tuning DBSCAN across various epsilon values, the conventional approach struggles to group radar detections into a single coherent cluster. As shown in Fig. 5a, at $\epsilon = 5$, only around 40% of frames yield exactly one cluster per frame, consistent with the single-target ground truth. This low accuracy highlights the challenges posed by glint noise in automotive radar data, often resulting in missegmentation into multiple small clusters.

To further assess the performance, we calculated the Euclidean distance between the centroid of the detected cluster and the ground truth centroid for frames with a single cluster (see Fig. 5b). These metrics underscore the need for improved clustering techniques. Despite the low overall success rate, when DBSCAN forms a single cluster, larger ϵ values remarkably tend to yield centroids closer to the ground truth. However, the Euclidean error remains high (approximately 7 meters). Even at the optimal ϵ for centroid accuracy, overall clustering performance is insufficient, and increasing ϵ beyond 5 is impractical due to merging distinct clusters and generating more false positives.

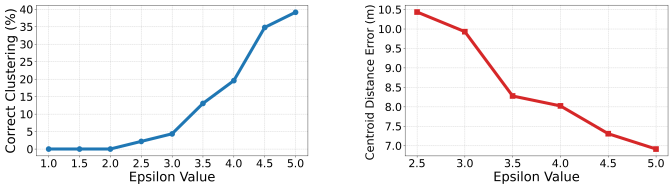

(a) (b)

Fig. 5: DBSCAN clustering performance: (a) percentage of correctly clustered frames for different ϵ values, and (b) distance between the correctly clustered clusters' mean and the ground truth.

B. Evaluation of IoU and Center Error

Fig. 6b illustrates the evolution over time of the center error, which is the Euclidean distance between the centroids of the estimated and ground truth bounding boxes. In the early frames, the error is noticeably high, probably due to factors such as glint noise, sparse detections when the truck

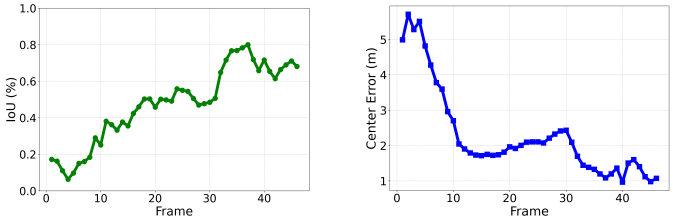

(a) (b)

Fig. 6: Tracking performance metrics: (a) IoU between estimated bounding boxes and ground truth, and (b) center error over frames.

first appears, and the radar's tendency to detect the closest point within its field of view, which is typically the front of the truck. As the tracker gathers more data and refines its estimates, the center error decreases remarkably, reflecting enhanced accuracy in pinpointing the true position of the target.

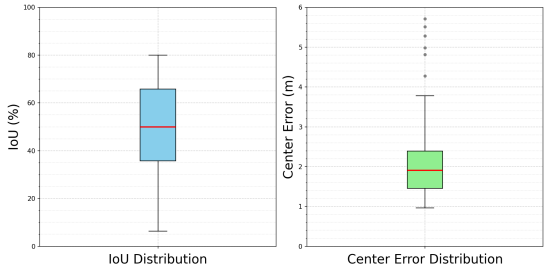

Fig. 7: Box plot illustrating the distribution of center error metric in meters, and the percentage of Intersection over Union (IoU).

In Fig. 7, a box-and-whisker plot summarizes the overall performance in terms of both IoU and center error. For most frames, the IoU values are high, meaning the estimated and actual bounding boxes overlap well. However, a few frames, mostly at the beginning, show lower IoU. This could be due to the early stages of tracking, as the tracker is still fine-tuning its heading estimation. Notably, even in these cases, the center error remains low, indicating that the primary issue stems from uncertainties in heading estimation rather than inaccuracies in size estimation.

Conversely, the center error distribution reveals a mean error of approximately 2.2 meters with a standard deviation of around 1.24 meters, suggesting that although certain frames exhibit larger errors, the majority of estimates remain within a meter or two of the ground truth centroid.

IV. Conclusion and Future Work

The findings in this paper highlight the need for a more reliable approach to radar-based vehicle tracking. The proposed method enhances clustering stability and tracking accuracy by incorporating target size estimation from the Range-Doppler map. In safety-critical applications such as traffic monitoring, where precise tracking of large vehicles is crucial, these enhancements help reduce the impact of glint noise on the tracker, increasing the tracking accuracy, and improving the overall reliability of the system. This approach will be extended in the future to incorporate multiple objects in the scene from a 2D Range-Doppler map.

References

[1] Hasch, J., Topak, E., Schnabel, R., Zwick, T., Weigel, R., & Waldschmidt, C., "Millimeter-wave technology for automotive radar sensors in the 77 GHz frequency band," *IEEE Transactions on Microwave Theory and Techniques*, vol. 60, no. 3, pp. 845–860, 2012, doi:10.1109/TMTT.2011.2178427

[2] Wenger, J., "Automotive radar–status and perspectives," in *2005 IEEE Compound Semiconductor Integrated Circuit Symposium*, pp. 4–7, 2005, doi:10.1109/CSICS.2005.1531741

[3] Patole, S. M., Torlak, M., Wang, D., & Ali, M., "Automotive radars: A review of signal processing techniques," *IEEE Signal Processing Magazine*, vol. 34, no. 2, pp. 22–35, 2017, doi:10.1109/MSP.2016.2628914

[4] Y. Zhang, X. Li, and M. Xing, "Maneuvering target tracking using IMMPF in Passive Coherent Location radar," in *Proceedings of the 2011 IEEE CIE International Conference on Radar*, Chengdu, China, Oct. 2011, pp. 1241–1244, doi:10.1109/CIE-Radar.2011.6159728

[5] D. M. Patterson and R. A. Ashley, "Glint Tracking Errors in Radar," in *A Nonlinear Time Series Workshop: A Toolkit for Detecting and Identifying Nonlinear Serial Dependence*, Boston, MA: Springer US, 2000, pp. 121–136, doi:10.1007/978-1-4419-8688-7.

[6] Bar-Shalom, Y., Li, X. R., & Kirubarajan, T., *Estimation with Applications to Tracking and Navigation: Theory Algorithms and Software*. John Wiley & Sons, 2001.

[7] A. Malacarne, F. Laghezza, F. Scotti, A. M. Tulino, A. Manna, and A. Bogoni, "Integrated multi-frequency lidar/radar system for precise and robust automotive applications," in *Proceedings of the 2015 IEEE International Conference on Microwaves, Communications, Antennas and Electronic Systems (COMCAS)*, Tel Aviv, Israel, Nov. 2015, pp. 1–5, doi:10.1109/RADAR.2015.7131160

[8] R. Murtaja, M. A. Raslan, T. Uhlich and A. Becker, "Comparison of Single Frame Classification with Micro-Doppler Classification of VRUs for Traffic Radar," in *2024 IEEE 13rd Sensor Array and Multichannel Signal Processing Workshop (SAM)*, Corvallis, OR, USA, 2024, pp. 1–8, doi:10.1109/SAM60225.2024.10636619

[9] A. Malacarne, F. Laghezza, F. Scotti, A. M. Tulino, A. Manna, and A. Bogoni, "Integrated multi-frequency lidar/radar system for precise and robust automotive applications," in *Proceedings of the 2015 IEEE International Conference on Microwaves, Communications, Antennas and Electronic Systems (COMCAS)*, Tel Aviv, Israel, Nov. 2015, pp. 1–5, doi:10.1109/TITS.2019.2950522

[10] B. Lorbeer, A. Kosareva, B. Deva, D. Softić, P. Ruppel, and A. Küpper, "Variations on the Clustering Algorithm BIRCH," *Big Data Research*, vol. 11, pp. 44–53, Mar. 2018, doi:10.1016/j.bdr.2017.09.002

[11] M. A. Raslan, M. Schmidhammer, F. de Ponte Müller, R. Murtaja, A. Becker, and T. Uhlich, "Robust Localization and Tracking of VRUs with Radar and Ultra Wide Band Sensors for Traffic Safety," SSRN preprint (under review), Oct. 2024. https://dx.doi.org/10.2139/ssrn.5004286

[12] Radar-Sensor.com, "Traffic Measurement Campaign in Project Videtec 2," 2024. [Online]. Available: https://radar-sensor.com/news/traffic-measurement-campaign-in-project-videtec-2.html, accessed Aug. 15, 2024.

[13] M. A. Richards, *Fundamentals of Radar Signal Processing*, 2nd ed. New York, NY, USA: McGraw-Hill, 2014.

[14] H. Rohling, "Radar CFAR thresholding in clutter and multiple target situations," *IEEE Transactions on Aerospace and Electronic Systems*, vol. AES-19, no. 4, pp. 608–621, Jul. 1983.

[15] A. Bewley, Z. Ge, L. Ott, F. Ramos, and B. Upcroft, "Simple online and realtime tracking," in *Proc. IEEE Int. Conf. Image Process. (ICIP)*, 2016, pp. 3464–3468, doi: 10.1109/ICIP.2016.7533003.

[16] R. E. Kalman,"A new approach to linear filtering and prediction problems," *Journal of Basic Engineering*, vol. 82, no. 1, pp. 35–45, 1960.